

## RESEARCH OUTPUTS / RÉSULTATS DE RECHERCHE

### Highly enhanced catalytic stability of copper by the synergistic effect of porous hierarchy and alloying for selective hydrogenation reaction

Yuan, Hao; Wang, Zhao; Jin, Shunjing; Xiao, Shanshan; Liu, Siming; Hu, Zhiyi; Chen, Lihua; Su, Baolian

*Published in:*  
Catalysts

*DOI:*  
[10.3390/catal12010012](https://doi.org/10.3390/catal12010012)

*Publication date:*  
2022

*Document Version*  
Publisher's PDF, also known as Version of record

[Link to publication](#)

*Citation for published version (HARVARD):*

Yuan, H, Wang, Z, Jin, S, Xiao, S, Liu, S, Hu, Z, Chen, L & Su, B 2022, 'Highly enhanced catalytic stability of copper by the synergistic effect of porous hierarchy and alloying for selective hydrogenation reaction', *Catalysts*, vol. 12, no. 1, 12. <https://doi.org/10.3390/catal12010012>

#### General rights

Copyright and moral rights for the publications made accessible in the public portal are retained by the authors and/or other copyright owners and it is a condition of accessing publications that users recognise and abide by the legal requirements associated with these rights.



- Users may download and print one copy of any publication from the public portal for the purpose of private study or research.
- You may not further distribute the material or use it for any profit-making activity or commercial gain
- You may freely distribute the URL identifying the publication in the public portal ?

#### Take down policy

If you believe that this document breaches copyright please contact us providing details, and we will remove access to the work immediately and investigate your claim.

## Article

# Highly Enhanced Catalytic Stability of Copper by the Synergistic Effect of Porous Hierarchy and Alloying for Selective Hydrogenation Reaction

Hao Yuan <sup>1,2</sup>, Zhao Wang <sup>1,2,\*</sup> , Shunjing Jin <sup>3</sup>, Shanshan Xiao <sup>2</sup>, Siming Liu <sup>2</sup>, Zhiyi Hu <sup>2</sup>, Lihua Chen <sup>2</sup> and Baolian Su <sup>2,4,\*</sup> 

- <sup>1</sup> Foshan Xianhu Laboratory of the Advanced Energy Science and Technology Guangdong Laboratory, Guangdong Laboratory, Xianhu Hydrogen Valley, Foshan 528200, China; 303934@whut.edu.cn
- <sup>2</sup> Laboratory of Living Materials, The State Key Laboratory of Advanced Technology for Material Synthesis and Processing, Wuhan University of Technology, Wuhan 430070, China; 303768@whut.edu.cn (S.X.); 317580@whut.edu.cn (S.L.); Zhiyi.hu@whut.edu.cn (Z.H.); chenlihua@whut.edu.cn (L.C.)
- <sup>3</sup> Xiangyang Polytechnic, Xiangyang 441050, China; 317150@whut.edu.cn
- <sup>4</sup> Laboratory of Inorganic Materials Chemistry (CMI), University of Namur, 61 Rue de Bruxelles, B-5000 Namur, Belgium
- \* Correspondence: zhao.wang@whut.edu.cn (Z.W.); bao-lian.su@unamur.be (B.S.)

**Abstract:** Supported copper has a great potential for replacing the commercial palladium-based catalysts in the field of selective alkynes/alkadienes hydrogenation due to its excellent alkene selectivity and relatively high activity. However, fatally, it has a low catalytic stability owing to the rapid oligomerization of alkenes on the copper surface. In this study, 2.5 wt% Cu catalysts with various Cu:Zn ratios and supported on hierarchically porous alumina (HA) were designed and synthesized by deposition–precipitation with urea. Macropores (with diameters of 1  $\mu\text{m}$ ) and mesopores (with diameters of 3.5 nm) were introduced by the hydrolysis of metal alkoxides. After in situ activation at 350  $^{\circ}\text{C}$ , the catalytic stability of Cu was highly enhanced, with a limited effect on the catalytic activity and alkene selectivity. The time needed for losing 10% butadiene conversion for Cu1Zn3/HA was  $\sim 40$  h, which is 20 times higher than that found for Cu/HA ( $\sim 2$  h), and 160 times higher than that found for Cu/bulky alumina (0.25 h). It was found that this type of enhancement in catalytic stability was mainly due to the rapid mass transportation in hierarchically porous structure (i.e., four times higher than that in bulky commercial alumina) and the well-dispersed copper active site modified by Zn, with identification by STEM–HAADF coupled with EDX. This study offers a universal way to optimize the catalytic stability of selective hydrogenation reactions.

**Keywords:** hierarchically porous structure; selective hydrogenation reaction; unsaturated hydrocarbons; copper–zinc alloy; synergistic effect; 1,3-butadiene



**Citation:** Yuan, H.; Wang, Z.; Jin, S.; Xiao, S.; Liu, S.; Hu, Z.; Chen, L.; Su, B. Highly Enhanced Catalytic Stability of Copper by the Synergistic Effect of Porous Hierarchy and Alloying for Selective Hydrogenation Reaction. *Catalysts* **2022**, *12*, 12. <https://doi.org/10.3390/catal12010012>

Academic Editor: Ivan V. Kozhevnikov

Received: 6 December 2021

Accepted: 21 December 2021

Published: 24 December 2021

**Publisher's Note:** MDPI stays neutral with regard to jurisdictional claims in published maps and institutional affiliations.



**Copyright:** © 2021 by the authors. Licensee MDPI, Basel, Switzerland. This article is an open access article distributed under the terms and conditions of the Creative Commons Attribution (CC BY) license (<https://creativecommons.org/licenses/by/4.0/>).

## 1. Introduction

Alkenes, especially  $\text{C}_2$ – $\text{C}_4$  olefins with a purity higher than 99.999%, are fundamental chemicals in the synthesis of polymers, surfactants and other products related to organic chemical industry by catalytic polymerization reactions [1]. In general, alkenes are mainly obtained from the hydrocracking of crude oil [2], which also results in small amounts of alkyne and diene impurities, such as 2–8% of propyne and propadiene in propene cuts [3] and 0.3–0.8% of butyne and butadiene in butenes cuts [4]. These impurities can poison the catalysts used for alkene polymerization and terminate the polymerization reaction by transforming catalysts to a stable intermediate [5,6]—i.e., 2-butyne and butadiene impurities react with  $\text{Cp}^*\text{ScCH}_3$  ( $\text{Cp}^* = \eta^5\text{-C}_5\text{Me}_5$ ) catalyst, forming a stable  $\text{Cp}^*\text{Sc}(\text{CH}_3)=\text{C}(\text{CH}_3)_2$  product [7]. Thus, the concentration of alkyne and diene impurities must be reduced to below 0.001%. The selective hydrogenation reaction, which can selectively convert the impurities into valuable alkene raw materials, is widely used in

industry. The classical catalyst for such reaction is the Lindlar catalyst [8], which consists of a palladium active site and a calcium carbonate support. However, in order to obtain a high alkene selectivity, the catalytic activity of the palladium is usually modified by some poison (e.g., lead, quinoline etc.). Moreover, noble-metal-based bi-metallic catalysts, e.g., Pd–Ag/Al<sub>2</sub>O<sub>3</sub> synthesized by the Süd-Chemie company [9–11], are the main commercial catalyst, but their high price (~USD 10,000 kg<sup>−1</sup>) and low selectivity to alkenes (<20% at full conversion) [12] largely limit their further utilization. Thus, the exploration of alternative catalysts with a high catalytic performance and low cost remains a great challenge in the current alkenes industry [13].

Copper is one of the best candidates for selective hydrogenation reactions due to its low cost and rather high catalytic activity and selectivity to alkenes. The price of copper-based catalysts is more than 1000 times lower than that of commercialized Pd-based catalysts. Compared with palladium-based catalysts, metallic Cu has shown a high selectivity to alkenes (>90% at full alkyne/diene conversion [14,15]) and moderate full alkyne/diene conversion temperature (75–150 °C [14–17]). In addition, copper has also shown an advanced catalytic property among non-noble metals [18] (e.g., Ni, Co, Fe) in terms of its selectivity to alkenes at full alkyne/diene conversion [19–21] and catalytic activity [22,23]. However, the main barrier to the commercialization of Cu catalysts is its rapid deactivation during selective hydrogenation reactions [24]. Specifically, mono-metallic copper supported on TiO<sub>2</sub> for the selective hydrogenation of butadiene has shown a butadiene conversion from 100% to below 20% in less than 3 h on stream [15], which is far from the requirement in industry. Numerous studies have focused on the exploration of deactivation mechanisms since the 1990s [25,26]. The loss of activity was mainly attributed to the coverage of catalytic active sites by the accumulation of foulants [5], which are C<sub>8</sub> to C<sub>22</sub> oligomers formed by the oligomerization of neighboring intermediate carbenes via metallocycles [27]. Developing Cu-based catalysts with a high catalytic stability is always a hot research topic in alkenes industry.

Tuning copper's active site could be an efficient way to obtain a high catalytic stability. By increasing the copper atom dispersion from 12.3% (i.e., nanoparticle) to 100% (i.e., atomic dispersion) on an alumina support, Lu et al. [16] observed an increase in the catalytic stability from 25 to 40 h for mono-metallic copper, with a decrease of the foulant accumulation from 30 wt% to 3.3 wt% during the acetylene hydrogenation reaction. A similar result was also verified by Ma et al. [17], who developed atomically dispersed Cu on nanodiamond–graphene that shows a stable acetylene conversion of 95% over 60 h of isothermal reaction. However, the synthesis of atomically dispersed Cu<sup>0</sup> remains a great challenge, as the Cu<sup>0</sup> atom is unstable and tends to be either aggregated into Cu nanoparticles or positively charged, by transferring electrons to its support (i.e., it shows a strong metal–support interaction). Alloying copper with other metal assistants [28] (e.g., Au [29], Pd [30–32], Pt [33] etc.) has been proposed to solve this drawback. Using a density functional theory calculation, Nørskov et al. [13] predicted that Cu–Zn alloy (e.g., Cu<sub>1</sub>Zn<sub>1</sub>) could be a potential replacement for current Pd-based catalysts. Recently, Louis et al. [34] experimentally verified that alloying Cu with small amounts of Zn (i.e., Cu<sub>3</sub>Zn<sub>1</sub> alloy and intermediate Cu<sub>0.9</sub>Zn<sub>0.1</sub> alloy) strongly improves the catalytic stability of Cu in the selective hydrogenation of butadiene, with butadiene conversion decreased from 100% to ~80% after 20 h of reaction for bi-metallic Cu–Zn catalysts. However, the specific surface area of the support is always a limitation, as it produces either a rather low Cu loading for atomically dispersed Cu catalysts or large metallic particles for Cu-based bi-metallic catalysts. Both decrease the apparent catalytic activity of supported Cu-based catalysts, with a high full alkyne/alkadiene conversion temperature.

Increasing the specific surface area of the support by introducing a porous structure shows great promise, as it could improve the Cu loading without affecting the Cu dispersion. For example, Ma et al. [35] synthesized ordered hierarchical porous silica (HPS), with a specific surface area above 600 m<sup>2</sup> g<sup>−1</sup> as the support for Cu catalysts. The supported Cu particles were confined to the porous structure, with a size smaller than 5 nm at 20 wt%

of Cu loading. The catalysts showed a rather high catalytic activity and stability in the hydrogenation of dimethyl adipate (i.e., a turnover frequency  $\sim 0.72 \text{ h}^{-1}$  and no decrease in dimethyl adipate conversion after 120 h of reaction). Moreover, they found the pore size in catalysts had a significant effect on the mass transportation of dimethyl adipate reactants and could limit the hydrogenation reaction. We have recently synthesized mono-metallic Cu supported by hierarchically porous carbon (HPC) with a Cu loading as high as 40–50 wt% by the in situ carbonization of HKUST-1 (with a surface area of  $1599 \text{ m}^2 \text{ g}^{-1}$ ) at a high temperature ( $>400 \text{ }^\circ\text{C}$ ) [36]. The special macro-mesoporous structure of the carbon support with well-confined Cu nanoparticles in Cu/HPC provided a rather high catalytic performance—i.e., butadiene conversion stayed at 100% for over 120 h of time on stream—showing that combining a porous hierarchy with a high surface area is an efficient way to improve the catalytic stability of mono-metallic Cu catalyst. However, the catalytic stability was still restricted by the utilization of mono-metallic Cu active sites, which could be further improved by the synthesis of Cu-based bi-metallic active sites on a hierarchically porous support.

Therefore, tuning the intrinsic properties of copper atoms by alloying on the surface of a hierarchically porous support could be a promising way to obtain a Cu-based catalyst with a highly enhanced catalytic stability. Compared with the previous carbon supports [36], alumina shows great advantages as a support for metallic catalysts due to its low cost and high thermal stability. Moreover, Louis et al. [34] mainly focused on Cu-rich bimetal Cu–Zn/TiO<sub>2</sub> catalysts that only produce Cu-rich Cu–Zn alloys, which are not highly consistent with the predictions (i.e., Cu1Zn1 alloy) of Nørskov et al. [13]. In this study, bi-metallic Cu–Zn catalysts with 2.5 wt% of Cu and an excess of Zn supported by hierarchically porous Al<sub>2</sub>O<sub>3</sub> were synthesized for the selective butadiene hydrogenation. Zn is inert for selective hydrogenation and acts as catalytic assistant. The study on the synergistic effect of a porous hierarchy and alloying on enhancing catalytic performance was carried out on the copper catalysts, with various Cu:Zn ratios and different porous structures. This study provides a powerful and universal way to optimize catalytic performance in both homogeneous and heterogeneous reactions.

## 2. Results and Discussion

### 2.1. Preparation of the Hierarchically Porous Alumina Supported Bimetallic Cu–Zn Catalysts

The hierarchically porous structure in the alumina support was self-constructed by the rapid hydrolysis and condensation of metal alkoxides in the absence of any templates (Figure 1). Specifically, once aluminum sec-butoxide (TBOA) was dropped into an aqueous solvent, it rapidly hydrolyzed to hydroxy-alumina, with the hydrolysis and condensation reaction as follows [37,38]:



Moreover, during the solidification of the hydroxy-alumina by the hydrolysis and condensation reaction, a large amount of sec-butyl alcohol (i.e., alcohol/Al molar ratio = 3) was rapidly formed and blow-off from the interior part of the TBOA toward the surrounding acetonitrile/water solvent. Meanwhile, the structure of the solid phase was modified by the fast fluxion of the sec-butyl alcohol, with an accumulation of the layered hydroxy-alumina (i.e., AlOOH) around the liquid sec-butyl alcohol [38,39]. Finally, after removing the liquid solvent phase by drying at  $60 \text{ }^\circ\text{C}$ , followed by calcination at  $550 \text{ }^\circ\text{C}$  in air for 3 h, a hierarchically porous structure was constructed with  $\gamma$ -Al<sub>2</sub>O<sub>3</sub> support, with XRD patterns presented in Figure S1. The morphology of the macropores was identified by SEM (Figure 1), which shows macropores with a diameter of  $1 \text{ }\mu\text{m}$  and a wall of layered  $\gamma$ -Al<sub>2</sub>O<sub>3</sub>.

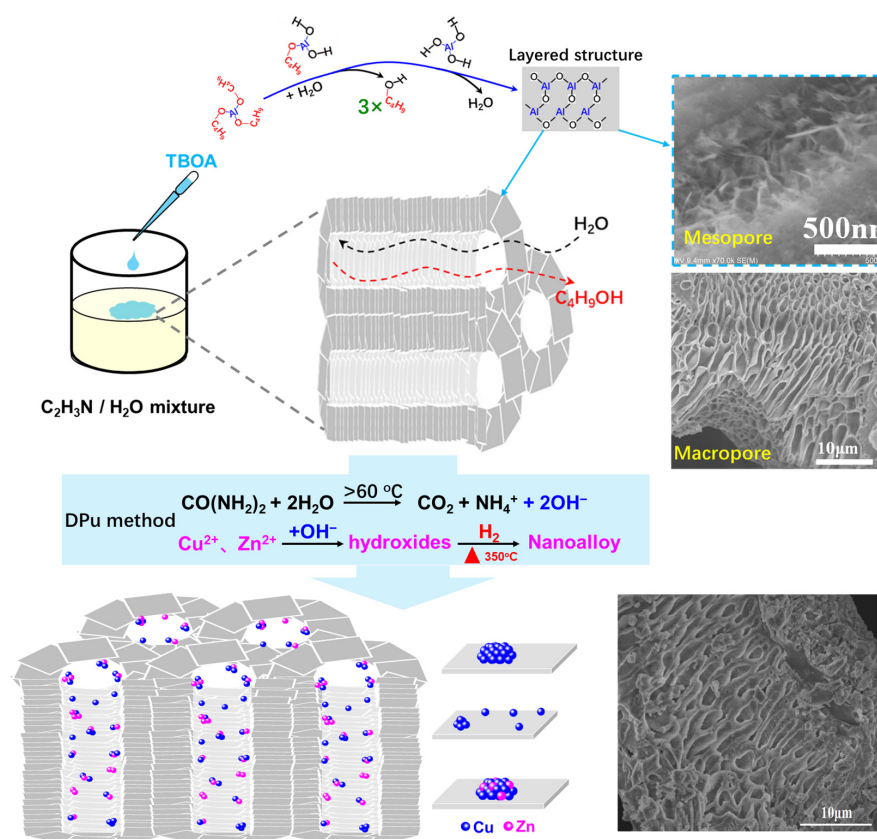


**Figure 1.** Illustration of the synthesis of a hierarchically porous alumina supported bi-metallic Cu–Zn catalyst.

The deposition–precipitation of  $Cu^{2+}$  and  $Zn^{2+}$  on the surface of hierarchically porous  $\gamma-Al_2O_3$  (HA) was realized by using urea as the precipitant. Urea, after dissolving in water, gradually decomposes at a temperature above  $60\text{ }^\circ C$ , with the formation of hydroxyl (i.e.,  $OH^-$ ). The increase of the  $OH^-$  concentration in solution promotes the deposition–precipitation of metal ions by the formation of hydroxides, and also by the modification of the surface charge of the support to create an electrostatic adsorption [40]. The metal loadings of Cu and Zn on HA are summarized in Table 1. A Cu loading of around 2.3 wt% was obtained for all the samples. As for the Cu1Zn1/HA, Cu1Zn3/HA and Cu1Zn5/HA samples, the Cu/Zn atomic ratios from our experimental analysis were 1:0.92, 1:2.3 and 1:3.6. The lower Zn loading than the nominal one was due to the higher solubility of zinc hydroxide ( $4.17 \times 10^{-17}\text{ mol L}^{-1}$ ) than that of copper hydroxide ( $2.0 \times 10^{-17}\text{ mol L}^{-1}$ ) [34]. Bi-metal Cu–Zn catalysts, with various Cu:Zn ratios, were successfully synthesized.

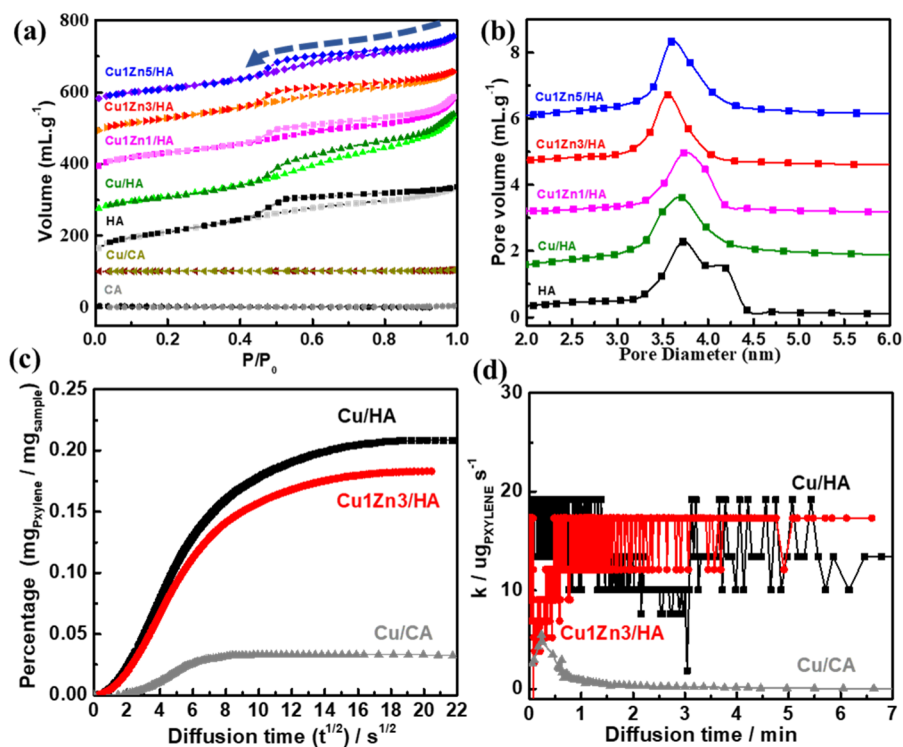
## 2.2. The Porous Hierarchy in Cu–Zn Supported on Hierarchically Porous $\gamma-Al_2O_3$

Figure 2a shows the nitrogen adsorption–desorption isotherms of all the prepared samples. Both HA and Cu–Zn/HA had a VI type of hysteresis loop in the relative pressures ( $P/P_0$ ) in the range of 0.4~1.0, indicating the presence of abundant mesopores in the samples. Based on the desorption behavior (dotted line in Figure 2a), the shape of the mesopores in the sample could be slits [41], formed by the stacking of the alumina nanosheet (Figure 1). Table 1 includes the textural properties of all the prepared samples. Specifically, the total surface area of pure HA was  $394\text{ m}^2\text{ g}^{-1}$ . The deposition of Cu–Zn by DPu brought a decrease in the total surface area to 355, 315, 291 and  $259\text{ m}^2\text{ g}^{-1}$  for Cu/HA, Cu1Zn1/HA, Cu1Zn3/HA and Cu1Zn5/HA, respectively. The mesopore distribution in the pure HA showed a main peak centered at 3.8 nm, with a shoulder at 4.2 nm (Figure 2b). After the deposition of Cu, the diameter of the mesopores slightly decreased to 3.7 nm. Moreover, with an increase of the Zn loading from 0 wt% to 5.3 wt%, the mesopore size

gradually decreased from 3.7 nm to 3.5 nm. In addition, the deposition of Cu brought a 15.7% decrease in the total pore volume of the HA: i.e.,  $0.57 \text{ cm}^3 \text{ g}^{-1}$  and  $0.48 \text{ cm}^3 \text{ g}^{-1}$  for HA and Cu/HA, respectively. As for Cu–Zn/HA, the total pore volume showed a 33.3% to 42% decrease with the increase of the Zn loading from 2.2 wt% to 5.3 wt%: i.e., 0.38 and  $0.33 \text{ cm}^3 \text{ g}^{-1}$  for Cu1Zn1/HA and Cu1Zn3/HA, respectively (Table 1). Specially, as for Cu1Zn5/HA, the dramatic decrease in the total surface area with an unchanged total pore volume and diameter indicate that the macroporous structure might have been slightly destroyed, as some fragments of alumina can be observed in SEM images (Figures S2 and S3). The decrease of the pore size and pore volume with the Cu–Zn loading indicates that the deposited Cu and Zn species were mainly located in the mesopores of the HA. The commercial alumina (CA) and Cu/CA showed no hysteresis loop, indicating their poorly porous nature. Moreover, the specific surface areas were 3 and  $4 \text{ m}^2 \text{ g}^{-1}$  for CA and Cu/CA, respectively. Thus, based on the characterization above, Cu–Zn/HA samples contained hierarchically macro–mesoporous structures, with macropore size of  $1 \mu\text{m}$  and mesopore size of 3.5 nm. Moreover, Cu and Zn were mainly deposited in the mesopores of the HA.

**Table 1.** Metal loadings and textural properties of as-prepared Cu–Zn/alumina catalysts.

Sample	Theoretical Values			Experimental Values			Total BET Surface Area ( $\text{m}^2/\text{g}$ )	Total Pore Volume ( $\text{cm}^3/\text{g}$ )	Meso Pore Diameter (nm)
	Loading (wt%)		Cu:Zn	Loading (wt%)		Cu:Zn			
	Cu	Zn		Cu	Zn				
HA	-	-	-	-	-	-	394	0.57	3.8, 4.2
Cu/HA	2.5	0	1:0	2.3	0	1:0	355	0.48	3.7
Cu1Zn1/HA	2.5	2.5	1:1	2.4	2.2	1:0.9	315	0.38	3.7
Cu1Zn3/HA	2.5	7.5	1:3	2.3	5.3	1:2.3	291	0.33	3.5
Cu1Zn5/HA	2.5	12.5	1:5	2.3	8.2	1:3.6	259	0.33	3.5
Cu/CA	2.5	0	1:0	2.3	0	1:0	4	-	-
CA	-	-	-	-	-	-	3	-	-



**Figure 2.**  $\text{N}_2$  adsorption–desorption isotherms (a) and pore size distribution curves (b) of Cu–Zn/ $\text{Al}_2\text{O}_3$  samples; the adsorption percentage (c) and the adsorption kinetic constant (d) of p-xylene as a function of diffusion time at  $50^\circ\text{C}$ .

The mass transportation accelerated by introducing a hierarchically porous structure into the alumina-supported copper catalyst was evaluated by the intelligent gravimetric analyzer (IGA) using *p*-xylene as the probe molecular. In this method, the probe molecular diffuses into the porous system and adsorbs onto the surface of materials, resulting in a weight increase. In Figure 2c, it can be found that the weight percentage of adsorbates on the Cu/bulky commercial alumina (Cu/CA) showed a slow increase to 0.05% in the first 6 s<sup>1/2</sup>, finally keeping constant at 0.05%. With a similar Cu loading, the weight percentage of adsorbates on Cu/HA rapidly increased above 0.12% in the first 6 s<sup>1/2</sup>, followed by a stabilization at 0.2%. Moreover, the addition of Zn slightly decreased the weight percentage of adsorbates; e.g., ~0.18% was observed for Cu1Zn3/HA. As for a constant material (i.e., alumina), the final weight of adsorbates was decided by the surface area of the samples. More importantly, the property of mass transportation in the samples was evaluated by the rate of the weight evolution as a function of the adsorption time. The adsorption kinetic constant (*k*) for these samples was calculated by the following formula [42] (Figure 2d):

$$m_{(t)} = m_0 - \Delta m[1 - \exp(-kt)] \quad (1)$$

where  $m_0$  is the weight of the sample (mg);  $m_{(t)}$  is the weight of the sample at time  $t$  during the test; and  $\Delta m$  is the weight increase after reaching the adsorption equilibrium. Figure 2d shows that the adsorption kinetic constant (*k*) for Cu/HA and Cu1Zn3/HA was 10~20  $\mu\text{g}_{\text{p-xylene}} \text{s}^{-1}$ , which was more than four times higher than that of CA (0~5  $\mu\text{g}_{\text{p-xylene}} \text{s}^{-1}$ ). It clearly indicates that, compared to bulky commercial alumina, the introduction of a hierarchically porous structure largely promotes the mass transportation of organic molecules in the sample.

### 2.3. The Property of Bimetallic Cu–Zn Supported on Hierarchically Porous $\gamma\text{-Al}_2\text{O}_3$

The reduction temperature for Cu–Zn/HA samples was chosen based on temperature-programmed reduction results (Figure 3a). A H<sub>2</sub> consumption peak was observed at 260 °C for mono-metal Cu/CA, while a slightly higher reduction temperature of around 267 °C was observed for mono-metal Cu/HA. The higher reduction temperature indicates a stronger interaction between Cu and hierarchically porous Al<sub>2</sub>O<sub>3</sub> in Cu/HA than that with Cu/CA. After the addition of Zn, the reduction temperature shifted to 269 °C for Cu1Zn1/HA. With an increasing Zn loading in bi-metal Cu–Zn/CA samples, the reduction temperature gradually increased to 292 °C and 310 °C for Cu1Zn3/HA and Cu1Zn5/HA, respectively. It is well known that mono-metal Zn has no reduction peak at any temperature lower than 550 °C [20]; the H<sub>2</sub> consumption peak is thus mainly due to the reduction of Cu<sup>2+</sup>. Furthermore, the high reduction temperature in bi-metal Cu–Zn/CA with an increase in the Zn loading indicates that a strong interaction existed between Cu and Zn. Finally, a reduction temperature of 350 °C was thus selected for the activation of all the samples.

After reduction at 350 °C for 2 h in H<sub>2</sub>, the state of the Cu and Zn phase was analyzed by X-ray diffraction patterns (Figure 3b). It shows a broad peak at around 46° for all the samples, which corresponds to the  $\gamma\text{-Al}_2\text{O}_3$  support (JCPDS: 01-1303). In addition, an additional peak appeared at around 43.3° in the reduced mono-metal Cu/HA sample, and it belongs to the (111) crystallite surface of metallic Cu (JCPDS card: 85-1326). After alloying Cu with Zn, a peak at ~43.3°, belonging to the (110) of Cu1Zn1 alloy, appeared in all bi-metal Cu–Zn/HA samples. Based on Scherrer's equation, the average particle size was calculated to be around 4 nm in the Cu/HA and Cu–Zn/HA samples. No peaks corresponding to Zn's phase were observed in any of the reduced Cu–Zn/HA samples. It was reported that the state of reduced Zn is difficult to identify by XRD, especially on a support [34]. The reduced Cu–Zn/HA samples were further analyzed by diffuse reflectance UV–vis spectroscopy (Figure 3c). The contribution of the support was firstly removed by using Al<sub>2</sub>O<sub>3</sub> as the baseline. Two absorption bands,  $\lambda_{\text{max}}$  ~270 nm and ~640 nm, were observed in the reduced mono-metal Cu/HA sample. These two bands are the characteristic bands of copper, and they are attributed to the localized surface plasmon resonance of free electrons and the inter-band transitions [43,44]. After alloying Cu with Zn, the characteristic bands

of metallic Cu, especially  $\lambda_{\max}$  in the visible region, showed a blue shift to 630 nm, 625 nm and 600 nm for Cu1Zn1/HA, Cu1Zn3/HA and Cu1Zn5/HA, respectively. This type of blue shift mainly originated from the electron transfer from Zn atoms to Cu, very probably due to the formation of Cu–Zn alloy (i.e., Cu1Zn1 alloy), which results in an increase in the density of free electrons in copper after reduction at 350 °C [45].

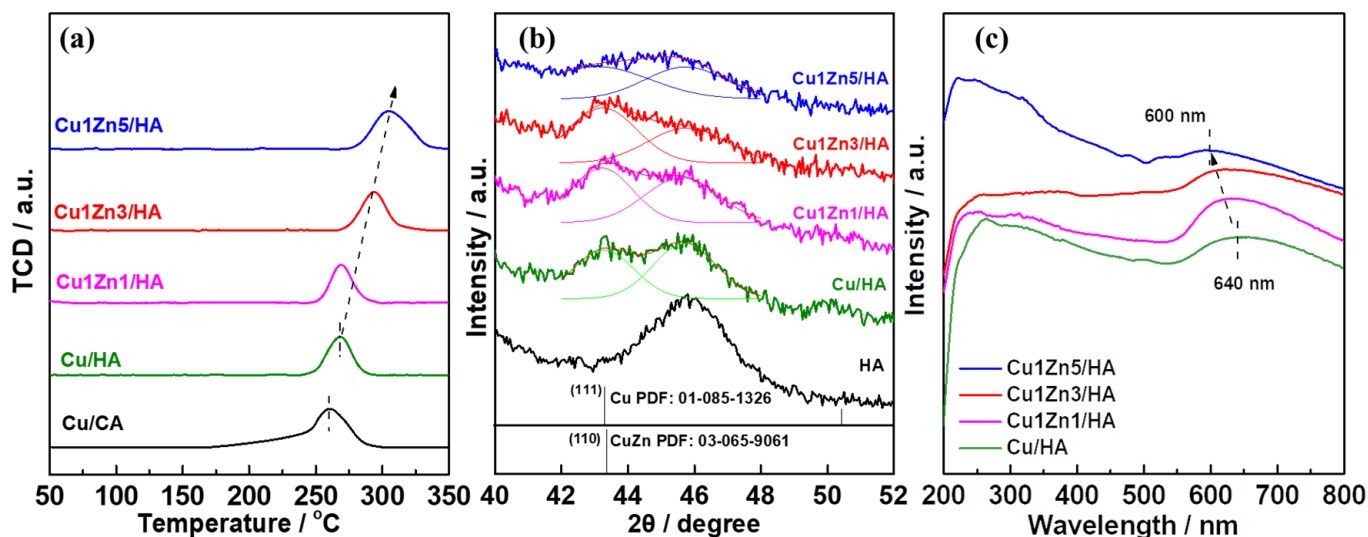


**Figure 3.** (a) Temperature programmed reduction of Cu–Zn/Al<sub>2</sub>O<sub>3</sub>; (b) XRD of Cu–Zn/Al<sub>2</sub>O<sub>3</sub> after reduction at 350 °C for 2 h; (c) UV–visible spectra of the calcined-reduced Cu–Zn/Al<sub>2</sub>O<sub>3</sub> samples with Al<sub>2</sub>O<sub>3</sub> as baseline.

To obtain further information about the composition and the particle size of the supported metallic nanoparticles, STEM–HAADF coupled with EDX was employed on the calcined then reduced mono-metal Cu/Al<sub>2</sub>O<sub>3</sub> and bi-metal Cu–Zn/Al<sub>2</sub>O<sub>3</sub> samples (Figure 4). The particle size of the Cu on the bulky commercial Al<sub>2</sub>O<sub>3</sub> support was around 15 ± 2 nm, while it dramatically decreased to around 1.7 ± 0.5 nm when the support was hierarchically porous Al<sub>2</sub>O<sub>3</sub> (Figure S4). The much higher surface area of HA (i.e., 394 m<sup>2</sup> g<sup>−1</sup>), being 130 times that of CA (3 m<sup>2</sup> g<sup>−1</sup>), offered a much better Cu dispersion at a similar Cu loading. In addition, compared to mono-metal Cu/HA, the additional Zn had a limited effect on the metal particle size, with the average particle sizes being 1.8 ± 0.3, 1.2 ± 0.5 and 2.2 ± 0.5 for Cu1Zn1/HA, Cu1Zn3/HA and Cu1Zn5/HA, respectively (Figure S4). The composition of the metallic particles was analyzed by EDX dotting, e.g., for the Cu1Zn3/HA sample in Figure 4f. Three large particles (with diameters of 4–5 nm) were found by STEM–HAADF. The atomic ratios between Cu and Zn in these particles were around 1:1. This confirms that the large metallic particles (4–5 nm) in the bi-metal Cu–Zn/HA were mainly Cu–Zn alloy; i.e., Cu–Zn with an atomic ratio of 1:1 was formed in the Cu1Zn3/HA sample. The excess of Zn was also identified by STEM–HAADF in Figure S5. Therefore, the observed XRD peak at 43° for bimetal Cu–Zn/HA was supposed to be the (110) crystallite surface of Cu1Zn1 alloy (JCPDS card: 65-9061) (Figure 3b). The small particles (<2 nm) in the Cu–Zn/HA samples were further analyzed by high resolution transmission electron microscopy with a double spherical aberration correction, e.g., for Cu1Zn3/HA sample in Figure 4g–i. With increasing magnification, sub-nanoclusters and automatically dispersed metallic atoms were mainly observed. According to the EDX mapping in Figure 4h, the metallic particles (~2 nm) contained metallic Cu, with small amounts of Zn. Automatically dispersed metallic atoms corresponded to Cu<sup>0</sup>. As a result, the TEM–EDX indicated that the bimetal Cu–Zn/HA samples mainly had Cu–Zn nanoalloy clusters, with plenty of atomically dispersed Cu.



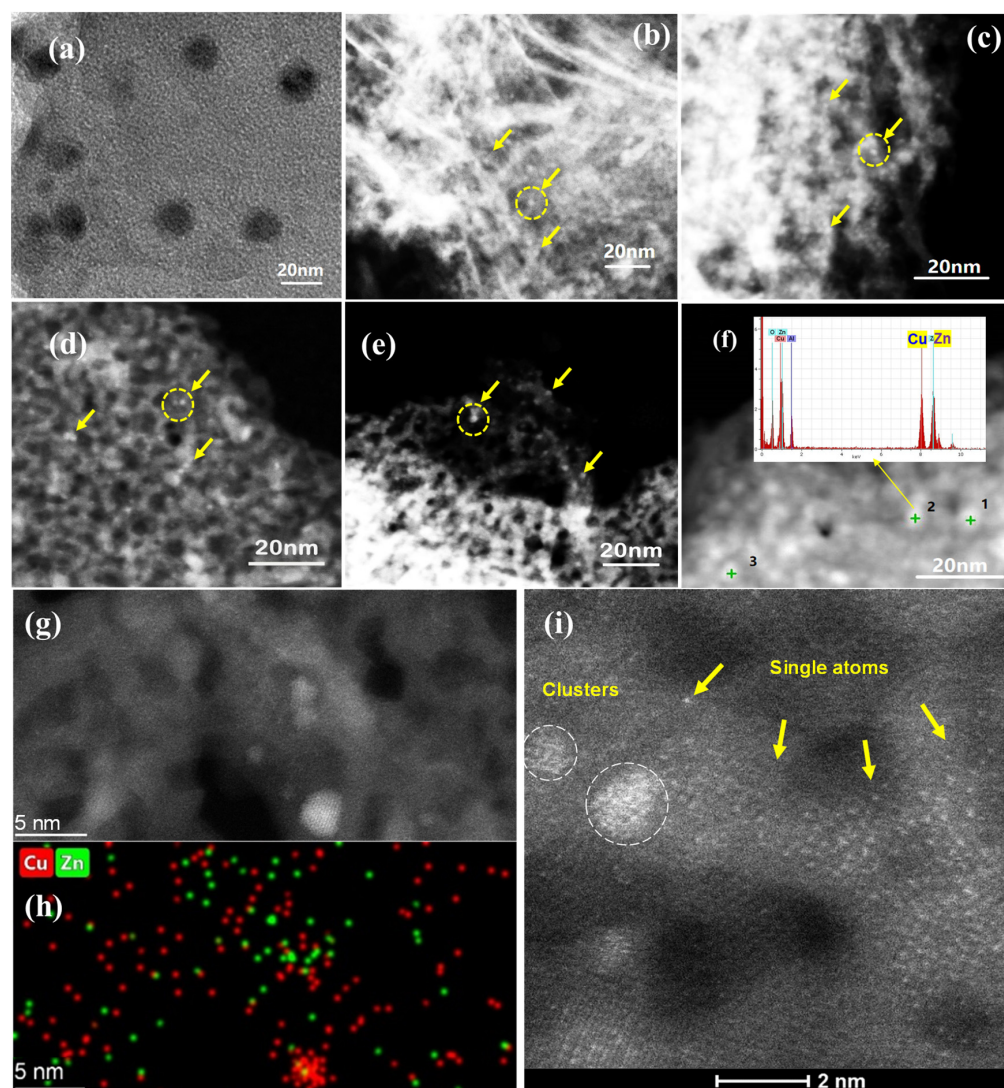


**Figure 4.** STEM of reduced Cu/CA (a), STEM-HAADF of reduced Cu/HA (b), Cu<sub>1</sub>Zn<sub>1</sub>/HA (c), Cu<sub>1</sub>Zn<sub>3</sub>/HA (d,g,i) and Cu<sub>1</sub>Zn<sub>5</sub>/HA (e); the EDX dotting (f) and mapping (h) of a Cu<sub>1</sub>Zn<sub>3</sub>/HA sample.

#### 2.4. Catalytic Performance for Selective Butadiene Hydrogenation in an Excess of Propene

After in situ reduction at 350 °C for 2 h under H<sub>2</sub>, the catalytic performance, including activity, alkene selectivity and stability, of the supported Cu–Zn samples for the selective hydrogenation of butadiene was evaluated (Figure 5) on 200 mg of each catalyst (sieve fraction, 125–200 μm), with similar Cu content (~2.5 wt%).

In Figure 5a, it can be seen that mono-metallic Cu supported on the bulky commercial Al<sub>2</sub>O<sub>3</sub> catalyst (Cu/CA) had a maximum butadiene conversion temperature ( $T_{\max}$ ) of around 200 °C, while the introduction of the porous hierarchy into Al<sub>2</sub>O<sub>3</sub> brought a decrease in the  $T_{\max}$  to ~175 °C for the Cu/HA. The enhanced activity in the Cu/HA resulted from both the smaller size of the supported Cu nanoparticles and the promoted mass transportation owing to the hierarchically porous structure in the HA support. However, in comparison with the previous study of Cu/TiO<sub>2</sub> ( $T_{\max}$  ~75 °C) [34], the high  $T_{\max}$  (i.e., low activity) of mono-metallic Cu supported on alumina might have been caused by the effect of different metal oxide supports owing to the metal–support interaction. Furthermore, the addition of zinc to the mono-metallic Cu/HA resulted in an increase in  $T_{\max}$ . With the increase in the Zn loading, the  $T_{\max}$  increased to 200, 220 and 230 °C for Cu<sub>1</sub>Zn<sub>1</sub>/HA, Cu<sub>1</sub>Zn<sub>3</sub>/HA and Cu<sub>1</sub>Zn<sub>5</sub>/HA, respectively. The lower catalytic activity (i.e., higher  $T_{\max}$ ) in the bi-metallic Cu–Zn/HA catalyst was caused by the less exposed Cu active sites in

CuZn alloy than those in the mono-metallic Cu, as Zn had no activity to the catalytic reaction. A similar observation on supported bi-metallic catalysts (i.e., Au–Zn [46], Pd–Zn [47], Cu–Zn [34] etc.) was previously reported. This result is also in good agreement with the theoretical prediction made by Nørskov [13] that Cu–Zn alloy has a lower activity than metallic Cu.

The catalytic selectivity of Cu–Zn catalysts is presented in Figure 5b. To simulate the real situation in industry (e.g., a butadiene impurity in an excess of butenes), 3000 ppm of butadiene in 30% of propene with helium as the balance gas was used as the raw materials in this study; thus, the catalytic selectivity could be expressed as both selectivity to butenes and alkanes (butane and propane) formation. In Figure 5b, it can be seen that the selectivity to butenes slightly decreased with the increase in the butadiene conversion; however, all Cu-based catalysts showed a high catalytic selectivity to butenes (i.e., >90%), with less than 10% alkane (butane and propane) formation. The advantage of the porous hierarchy can be clearly observed by comparing the alkene selectivity between Cu/CA and Cu/HA. Specifically, Cu supported on hierarchically porous Al<sub>2</sub>O<sub>3</sub> showed a higher selectivity to alkenes than did commercial bulky Al<sub>2</sub>O<sub>3</sub>. With the butadiene conversion increased from 20 to 100%, the butene selectivity decreased from 100% to ~97% and from 98.5% to ~90% for Cu/HA and Cu/CA, respectively. The superior alkene selectivity of Cu/HA was mainly due to the rapid guest molecule diffusion in Cu/HA (Figure 2d) shortening the residence time of the reactants over the copper's active site, avoiding the over-hydrogenation of butenes during the catalytic reaction [48]. In addition, the promotional effect of alloying Cu with Zn was checked by analyzing the alkene selectivity of Cu–Zn/HA catalysts. The alkene selectivity of bi-metallic Cu–Zn/HA stayed above 97% at ~100% butadiene conversion (e.g., ~99% alkene selectivity for Cu<sub>1</sub>Zn<sub>3</sub>/HA) as the modified electronic structure of the copper site by the formation of Cu–Zn alloy (Figure 3c). Even though the previous Cu–Zn/TiO<sub>2</sub> study [34] showed a decrease in the butene selectivity at 100% butadiene conversion after alloying Zn with Cu, it attributed this type of decrease in the alkene selectivity to a gradual deactivation of the mono-metallic copper during the slow heating ramp. In this study, the developed Cu–Zn/HA catalysts were stable enough (as discussed later); it is able to show a clear advantage of Zn for enhancing the alkene selectivity of Cu. Moreover, compared with Cu/CA, the Cu–Zn/HA catalysts showed a much higher selectivity to butenes, especially at a high butadiene conversion. For example, the Cu<sub>1</sub>Zn<sub>3</sub>/HA samples had an alkane (butane and propane) formation of ~2%, which was four times lower than that of Cu/CA sample, at a butadiene conversion close to 100%. This type of highly improved selectivity was indeed due to the synergistic effect of the rapid mass transportation and modified property of active site.

Butadiene conversion as a function of the time on stream was evaluated on Cu–Zn/Al<sub>2</sub>O<sub>3</sub> samples and presented in Figure 5c, with a similar initial butadiene conversion of ~60%. The reference catalyst (i.e., Cu/CA) had a very low catalytic stability and its butadiene conversion rapidly decreased from 60% to below 20% in the first 2 h of isothermal reaction. However, the butadiene conversion remained relatively stable for the mono-metallic Cu supported on HA, which showed a slight decrease to ~35% after 70 h of time on stream. This type of enhancement in the catalytic stability in the Cu/HA catalyst could be mainly due to the introduced hierarchically porous structure, which highly accelerated the mass transportation and improved the copper's dispersion, leading to an increase in the reactant transfer on the surface of the Cu's catalytically active site. Previous studies proved that the formation of oligomers (i.e., C<sub>8</sub> to C<sub>22</sub>) by the oligomerization of neighboring intermediate carbenes is the main reason for the deactivation of supported metal [27]. Moreover, Louis et al. [49] verified that the decomposition of oligomers mainly happens at temperatures lower than 450 °C by thermo-gravimetry coupled with mass spectra analysis. Here, the oligomers formation on Cu catalysts after a stability test was evaluated by thermo-gravimetry analysis in air (Figure S6). The weight loss of the Cu/CA and Cu/HA was 5.4 wt% and 4 wt%, respectively. It indicates that the rapid reactants transportation in the porous hierarchy brought a low oligomer formation, hence a slower deactivation rate.

The addition of Zn to Cu highly improved the catalytic stability of Cu in the selective hydrogenation reaction. In the first 70 h of reaction, the butadiene conversion decreased from 60% to 45% and 50% for Cu1Zn1/HA and Cu1Zn3/HA, respectively. However, it decreased from 60% to ~25% for the Cu1Zn5/HA sample. These are much more stable results than the previous Cu–Zn/TiO<sub>2</sub> catalysts (Cu:Zn < 1:1) [34], which had above 20% of deactivation in 20 h of time on stream. Moreover, this work also proposed a suitable Zn loading range (Cu:Zn ≈ 1:3) for bi-metallic Cu–Zn catalysts for the selective hydrogenation reaction. Based on the ICP, XRD and EDX characterization, two types of zinc existed in the bi-metallic Cu–Zn catalysts. One was that alloyed with Cu and another one was highly dispersed on the Al<sub>2</sub>O<sub>3</sub> support, and the distribution of Zn was imaged by EDX mapping in Figure S5. The main function of the Zn that alloyed with Cu was its modification of the adsorption mode or strength of the reactants and/or products of the reaction as it was reported in a previous bi-metallic Cu–Zn study [34], resulting in a decrease of green oil formation (Figure S6), e.g., only a 2.5 wt% weight loss for Cu1Zn3/HA. The positive role of Zn in Ni–Zn alloy was recently explored in the selective hydrogenation of acetylene, and it was found that alloying Zn with Ni could decrease the resultant coverage of acetylene, and weaken the carbon chain growth reaction (oligomerization reaction) [27]. This was attributed to changes in the electronic properties of Ni on the surface by alloying with Zn [13]. The same effect might also apply to the case of the Cu–Zn system, as a recent study based on DFT calculations found the existence of a charge transfer between the Cu and Zn atoms in Cu<sub>0.7</sub>Zn<sub>0.3</sub> alloy [50]. In addition to the modification of the electronic properties of Cu, alloying with Zn also brought a geometric effect. Zn had no catalytic activity in butadiene hydrogenation; alloying Zn with copper was supposed to dilute the Cu catalytic active site, and increase the average distance between Cu active sites on the surface of nano metallic particles. As it was presented in Figure S7, the crystal structure of metallic Cu and Cu1Zn1 shows that, as for mono-metallic Cu, the distance between neighboring Cu was around 2.5562 Å, which was shorter than the length of the butadiene molecular size (3.556 Å). After alloying with Zn, the distance between two copper atoms enlarged to 3.959 Å. Since the oligomerization reaction on a catalytic surface requires a sufficiently short distance between the co-adsorbed hydrocarbon molecules [51], the isolation of Cu by alloying with Zn could also avoid undesired side reactions for green oil formation. A similar geometric effect has also been observed in the bi-metallic Ni–Cu system; the isolated Ni–Cu sites showed larger coupling barriers to C–C bond formation than pure Ni or Cu sites owing to the alloy structure offering a high resistance to the formation of oligomers during propyne hydrogenation [52]. The fraction of zinc that is un-alloyed with copper on an Al<sub>2</sub>O<sub>3</sub> surface may modify the surficial acidic property of Al<sub>2</sub>O<sub>3</sub> [34], as the acidic sites on the support surface could adsorb hydrocarbons and provoke not only isomerisation but also transformation into coke or C<sub>2</sub>–C<sub>6</sub> hydrocarbons from cracking and disproportionation reactions [5,53].

Once both the hierarchically porous structure and Cu alloyed with Zn were simultaneously introduced into Cu/Al<sub>2</sub>O<sub>3</sub>, a great enhancement in the catalytic stability can be also observed in Figure 5c. More specifically, to make a fair comparison, the time taken to reach a 10% loss of the butadiene conversion was selected from Figure 5c and summarized in Figure 6a. Cu/CA showed a 10% butadiene conversion loss within 0.25 h, while that time was ~2 h, 5 h, 40 h and 10 h for Cu/HA, Cu1Zn1/HA, Cu1Zn3/HA and Cu1Zn5/HA, respectively. This indicates that Cu1Zn3/HA had a catalytic stability 20 times higher than that of Cu/HA, and 160 times higher than that of Cu/CA. As a result, the catalytic synergism between a porous hierarchy and alloying could offer a high-efficiency mass transportation and highly dispersed catalytically active site that results in a long-term catalytic reaction (Figure 6b).

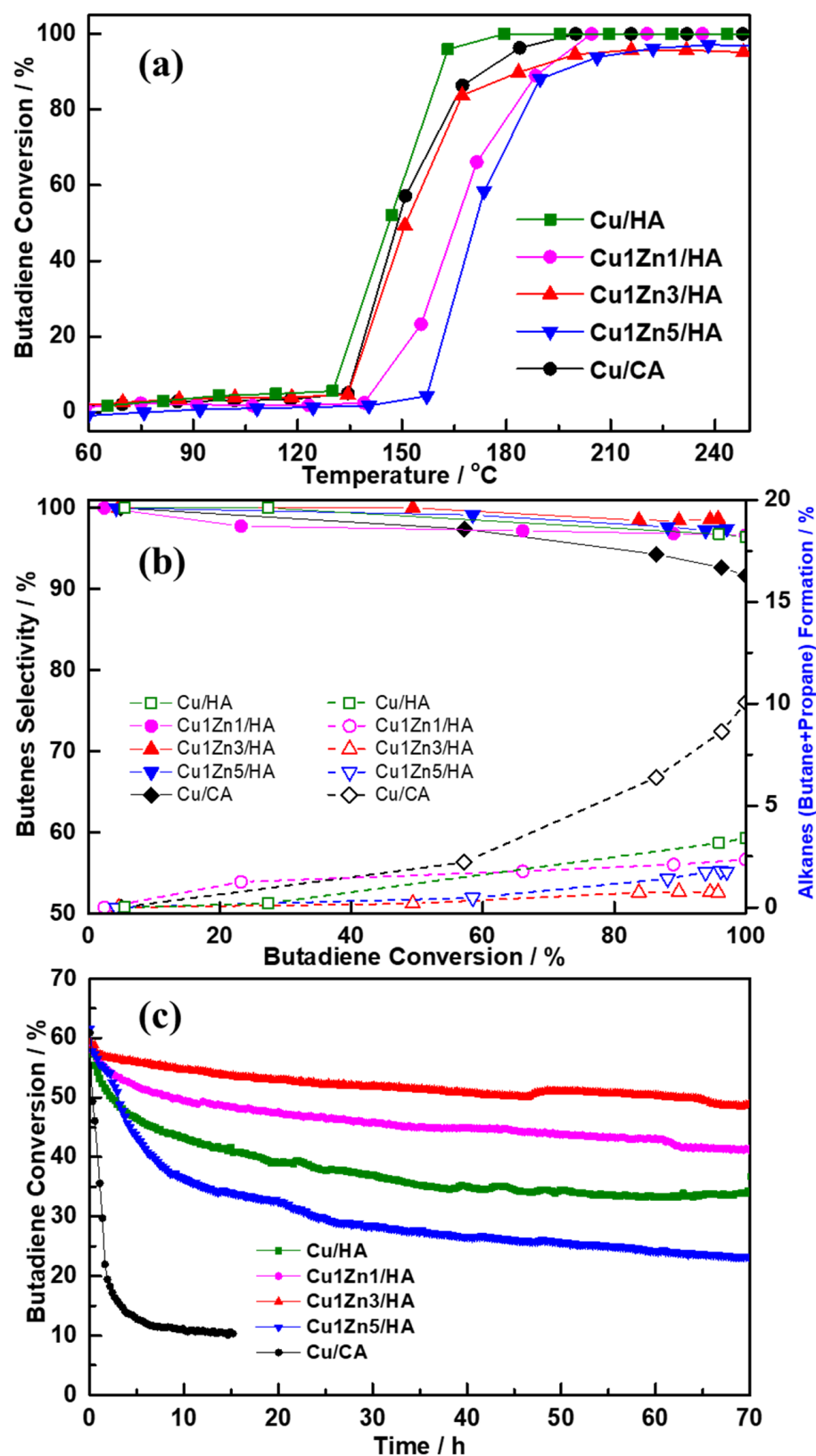
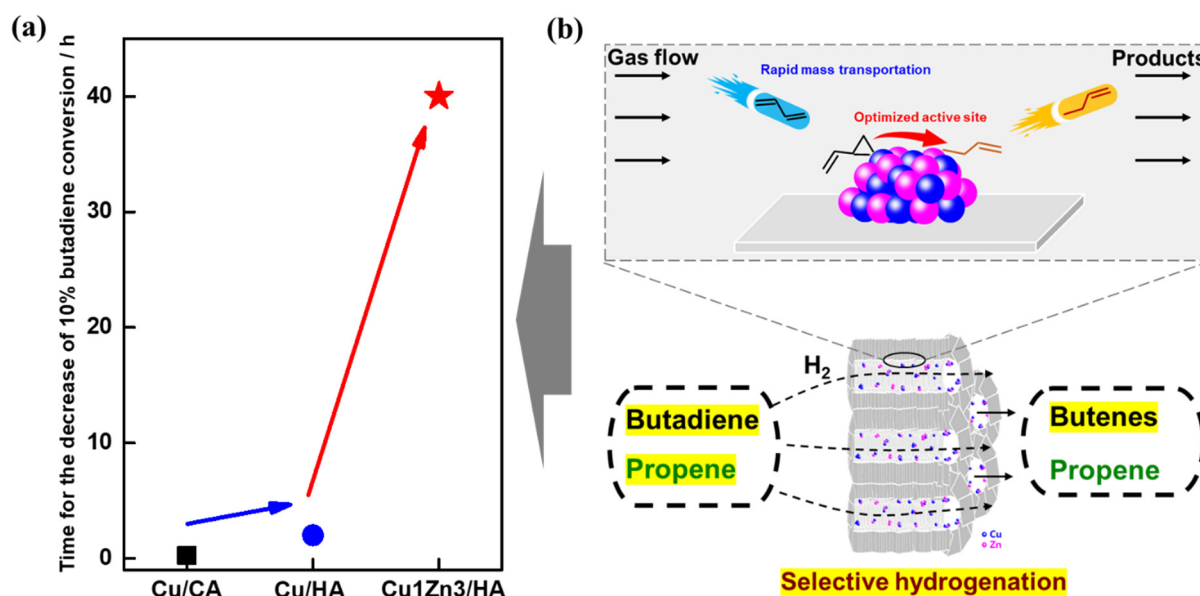


Figure 5. Evolution of the butadiene conversion as a function of reaction temperature (a); the selectivity to butenes (1-butene + cis-2-butene + trans-2-butene) and alkane formation as a function of butadiene conversion (b); butadiene conversion as a function of time on stream (c) for Cu-Zn/Al<sub>2</sub>O<sub>3</sub> catalysts (i.e., 150 °C for Cu/CA and Cu/HA; 175 °C for Cu1Zn1/CA and Cu1Zn5/HA; and 160 °C for Cu1Zn1/CA).



**Figure 6.** Evolution of the time needed to reach a 10% butadiene conversion decrease with different structures and compositions of samples (a) and a scheme of the synergistic effect of porous hierarchy and alloying in a catalytic reaction (b).

### 3. Experiment

#### 3.1. Sample Preparation

##### 3.1.1. Materials and Chemicals

The chemicals used were acetonitrile (Aladdin, ACS, 99.4%, Shanghai, China), aluminum sec-butoxide (Aladdin, 97%, Shanghai, China), distilled water,  $\text{Cu}(\text{NO}_3)_2 \cdot 3\text{H}_2\text{O}$  (Sinopharm, AR, Shanghai, China),  $\text{Zn}(\text{NO}_3)_2 \cdot 6\text{H}_2\text{O}$  (Sinopharm, AR, Shanghai, China) and urea (Sinopharm, AR, Shanghai, China). All were used as purchased during the whole sample synthesis procedure.

##### 3.1.2. Preparation of Hierarchically Porous Alumina

Hierarchically porous alumina (HA) was synthesized by a one-step method in the absence of any templates. In a typical preparation process, 3 mL of distilled water was dropped into 17 mL of acetonitrile under stirring at room temperature for 30 min. A mass of 2 g of aluminum sec-butoxide (TBOA) was dropped into the above solvent without stirring, and the suspension was statically kept at room temperature for 30 min. The precipitate was collected by filtration and dried at 60 °C for 1 day. Calcination at 550 °C under air for 3 h with a ramp rate of 2 °C min<sup>-1</sup> was performed, leading to the formation of HA support.

##### 3.1.3. Preparation of Cu–Zn/HA Catalysts

HA-supported mono-metal Cu and bi-metal Cu–Zn catalysts were prepared by deposition–precipitation with urea (DPu) as previously described [54,55]. Specifically, 2 g of HA support was dispersed in 200 mL of distilled water in a double-walled reactor ( $m_{\text{HA}}/V_{\text{water}} = 1:100$ ) at room temperature. The pre-defined weight of  $\text{Cu}(\text{NO}_3)_2 \cdot 3\text{H}_2\text{O}$  and  $\text{Zn}(\text{NO}_3)_2 \cdot 6\text{H}_2\text{O}$  were added into the suspension to achieve a desired nominal copper loading with various Cu:Zn atomic ratios of 1:0, 1:1, 1:3 and 1:5. Urea was dissolved in the above suspension to achieve a urea-to-metal molar ratio of ca. 100. The mixture was kept at 80 °C for 20 h under a mild stirring. The solid sample was collected by centrifugation and subsequently washed with distilled water and centrifuged three times. Finally, the solids were dried at 60 °C overnight and calcined in a muffle furnace at 400 °C for 2 h with a heating rate of 5 °C min<sup>-1</sup> (as prepared).

For comparison, bulky commercial  $\text{Al}_2\text{O}_3$  (CA, Aladdin, CAS: 1344-28-1, size of 200 nm) was also used as a support. Note that the CA reference must have a large particle size,

which could lead to porous structure formation during sample post-treatment (e.g., drying, sieving etc.). CA-supported mono-metallic Cu was synthesized through the same DPu procedure described above.

In this study, the nominal Cu loading in all samples was kept at 2.5 wt%. Specifically, Cu/HA and Cu/CA corresponded to mono-metal Cu deposited on HA and CA, respectively. While, Cu<sub>1</sub>Zn<sub>1</sub>/HA, Cu<sub>1</sub>Zn<sub>3</sub>/HA and Cu<sub>1</sub>Zn<sub>5</sub>/HA corresponded to bi-metal Cu–Zn deposited on HA support, with nominal Cu:Zn atomic ratios of 1:1, 1:3 and 1:5, respectively.

### 3.2. Catalysts Characterization

Metal loadings in the as-prepared samples were analyzed for their contents and relative ratios of Cu to Zn in different catalysts by inductively coupled plasma spectrometry (ICP; Lehman-Merbu, Prodigy 7). The wavelength range was 165 to 1100 nm.

The reduction behavior of the supported metals was checked by temperature programmed reduction under 5% H<sub>2</sub>/Ar atmosphere (H<sub>2</sub>-TPR; Micromeritics, AutoChem1 II 2920) using 100 mg of as-prepared samples. An Ar purge (25 mL min<sup>−1</sup>) was performed for 30 min to remove the air in the reactor at room temperature (RT) before increasing the temperature from room temperature to 550 °C at a linear rate (7.5 °C min<sup>−1</sup>) in a 5% H<sub>2</sub>/Ar gas mixture flow (25 mL min<sup>−1</sup>).

The crystalline structures of samples were determined by powder X-ray diffraction (XRD; Bruker D8 Advance, Cu K $\alpha$  radiation; 40 kV and 30 mA) with a scan rate of 0.5° min<sup>−1</sup>. The 2-theta angle ranged from 5° to 90°.

Surface morphology and metallic particle size were analyzed by scanning electron microscope (SEM; Hitachi, S-4800, Tokyo, Japan) equipped with energy dispersive X-ray spectrometer (EDX), and STEM–HAADF was performed on the machine Talos F200S (Thermo Fisher Scientific, Waltham, MA, USA). Moreover, single atomic Cu dispersion was analyzed by spherical-aberration-corrected transmission electron microscope (TEM; Tian G260-300, 200 kV, Thermo Fisher Scientific, Waltham, MA, USA). Statistical analysis of the nanoparticle size distributions in the reduced samples was obtained by counting more than 200 particles using the software Image J. The average particle diameter was deduced from the equation  $d_m = \sum n_i d_i / \sum n_i$ , where  $n_i$  is the number of the particles of diameter  $d_i$ .

Nitrogen adsorption–desorption isotherms were collected at 77 K with an ASAP-3020 (Micromeritics, Norcross, GA, USA) surface area analyzer manufactured by Micromeritics. The surface area was calculated from the adsorption branch using the Brunauer–Emmett–Teller (BET) method, and the pore size distribution was obtained based on the desorption branch with the Barrett–Joyner–Halenda (BJH) approach.

The mass transportation behavior in the hierarchically porous structure was evaluated by intelligent gravimetric analyzer (IGA, Hiden ISOHEMA Ltd., IGA100B, Hiden Isochema, Warrington, UK) using p-xylene as the probe molecular at 50 °C under ambient pressure. The weight of each sample was recorded every 0.12 s during p-xylene diffusion and adsorption.

The thermo-gravimetry analysis (TGA) was carried out on a thermogravimetric analyzer (Setaram Labsys Evo TGA-50, Setaram, Caluire-et-Cuire, France) from 150 to 450 °C in air with heating rate of 7.5 °C min<sup>−1</sup>.

### 3.3. Butadiene Selective Hydrogenation Reaction

The selective hydrogenation reaction was performed in a plug flow microreactor (inner diameter, 4 mm) either for the temperature programmed reaction (TP-reaction) or isothermal reaction under atmospheric pressure. To simulate the real situation in industry, which contains small amount of alkadiene impurities in alkenes, butadiene (0.3%) with an excess of propene (30%) was employed as the unsaturated hydrocarbons mixture in this study. The use of propene instead of butene made the butadiene hydrogenation products (i.e., butenes and butane) easily identifiable by gas chromatography; moreover, propene and butenes have a similar reactivity on the surface of metallic Cu [54], resulting

in no side effect on the catalytic reaction from the introduction of propene. Specifically, 200 mg of ex situ calcined catalyst (sieve fraction, 125–200  $\mu\text{m}$ ) was activated in situ under pure  $\text{H}_2$  (at 50  $\text{mL min}^{-1}$ ) from RT to 350  $^\circ\text{C}$  (at 2  $^\circ\text{C min}^{-1}$ ) and kept for 2 h at final temperature. After the reactor cooled down to room temperature under  $\text{H}_2$ , a mixture consisting of  $\sim 0.3\%$  butadiene, 20% hydrogen and 30% propene in He carrier was introduced with a total flow rate of 100  $\text{mL min}^{-1}$ . In the case of the temperature programmed reaction, the catalytic reaction was carried out from 30  $^\circ\text{C}$  to 300  $^\circ\text{C}$  with a heating rate of 1  $^\circ\text{C min}^{-1}$ . The concentration of reactants and target products was evaluated on-line by gas chromatography (GC2030Smart, FID detector, Tetvco, Wuhan, China) every 16 min, and thus every 16  $^\circ\text{C}$ . In the case of the isothermal reaction, the reaction was carried out directly after cooling down the oven to the testing temperature. The catalytic performance was recorded and studied as a function of time on stream for 70 h.

#### 4. Conclusions

In summary, a highly enhanced catalytic stability of supported copper was achieved by the synthesis of hierarchically porous- $\text{Al}_2\text{O}_3$ -supported bi-metallic Cu–Zn catalysts. The hierarchically porous  $\text{Al}_2\text{O}_3$ , which was synthesized by a “one drop” self-formation method, had a macro–mesoporous structure with pore diameters 1  $\mu\text{m}$  and 3.5 nm, respectively. After calcination then reduction at 350  $^\circ\text{C}$  for 2 h, Cu–Zn nanoalloys ( $\sim 4$  nm), bi-metallic Cu–Zn clusters ( $< 2$  nm) and atomically dispersed copper were found in bi-metallic Cu–Zn/HA catalysts. The catalytic performance was evaluated by the selective hydrogenation of butadiene in an excess of propene, and it was found that the hierarchically porous structure largely improved the catalytic stability; i.e., the hierarchically porous- $\text{Al}_2\text{O}_3$ -supported Cu catalyst had a much higher stability (with a  $\sim 25\%$  decrease in conversion after 70 h of reaction) than bulk- $\text{Al}_2\text{O}_3$ -supported Cu (with a  $\sim 50\%$  decrease in conversion after 10 h of reaction), and with a similar catalytic activity and selectivity. Alloying Cu with Zn slightly decreased the catalytic activity of Cu, but offered a high catalytic selectivity and stability. Moreover, the synergistic effect between the porous hierarchy and alloying could be clearly observed in the hierarchically porous- $\text{Al}_2\text{O}_3$ -supported bi-metallic Cu–Zn catalysts. Specifically, i.e., Cu<sub>1</sub>Zn<sub>3</sub>/HA (e.g., Cu<sub>1</sub>Zn<sub>1</sub> alloy) had a catalytic stability 20 times higher than that of Cu/HA and 160 times higher than that of Cu/CA. This study also reveals that the introduction of both a porous hierarchy structure and catalytic promoter by alloying could be an efficient way to improve the catalytic performance of other catalysts.

**Supplementary Materials:** The following supporting information can be downloaded at: <https://www.mdpi.com/article/10.3390/catal12010012/s1>, Figure S1: XRD of as-prepared and calcined hierarchically porous alumina; Figure S2: SEM of HA (a), Cu/HA(b), Cu<sub>1</sub>Zn<sub>1</sub>/HA(c), Cu<sub>1</sub>Zn<sub>3</sub>/HA(d), Cu<sub>1</sub>Zn<sub>5</sub>/HA(e) and Cu/commercial bulky alumina(f); Figure S3: SEM-EDS of Cu/HA, Cu<sub>1</sub>Zn<sub>1</sub>/HA, Cu<sub>1</sub>Zn<sub>3</sub>/HA and Cu<sub>1</sub>Zn<sub>5</sub>/HA; Figure S4: Particle size distribution. (a) Cu/CA; (b) Cu/HA; (c) Cu<sub>1</sub>Zn<sub>1</sub>/HA; (d)Cu<sub>1</sub>Zn<sub>3</sub>/HA; (e) Cu<sub>1</sub>Zn<sub>5</sub>/HA after calcination at 400  $^\circ\text{C}$  for 2h then reduction at 350  $^\circ\text{C}$  for 2h; Figure S5: STEM-HAADF coupled with EDS on the reduced Cu<sub>1</sub>Zn<sub>3</sub>/HA; Figure S6: TG analysis of Cu/CA and Cu–Zn/HA samples after stability test; Figure S7: The (111) and (110) crystal surface of metallic Cu (JCPDS:85-1326) and Cu–Zn alloy (JCPDS:65-9061).

**Author Contributions:** Conceptualization, B.S. and Z.W.; methodology, S.X., formal analysis, S.L., data interpretation, H.Y. and S.J., STEM-HAADF analysis, Z.H., Project administration, Z.W.; writing–review and editing, Z.W., B.S. and L.C.; funding acquisition, Z.W., B.S. and L.C. All authors have read and agreed to the published version of the manuscript.

**Funding:** This research was funded by the National 111 project of 2020 (B0002), Innovative Research Team (IRT\_15R52) of the Chinese Ministry of Education, the National Natural Science Foundation of China (NSFC-21902122), the Postdoctoral Science Foundation of China (grant 2019M652723), National Key R&D Program of China (grant 2021YFE0115800), the Foshan Xianhu Laboratory of the Advanced Energy Science and Technology Guangdong Laboratory (XHD2020-002) and the Joint Funds of the National Natural Science Foundation of China (grant U20A20122).

**Acknowledgments:** Zhao Wang thanks Catherine LOUIS, Laurent DELANNOY and Xue-Yu LI for data discussion.

**Conflicts of Interest:** The authors declare no conflict of interest.

## References

1. Corma, A.; Corresa, E.; Mathieu, Y.; Sauvanaud, L.; Al-Bogami, S.; Al-Ghrami, M.S.; Bourane, A. Crude oil to chemicals: Light olefins from crude oil. *Catal. Sci. Technol.* **2017**, *7*, 12–46. [[CrossRef](#)]
2. Marcilly, C. Evolution of refining and petrochemicals: What is the place of zeolites. *Oil Gas Sci. Technol.* **2001**, *56*, 499–514. [[CrossRef](#)]
3. Derrien, M.L. Chapter 18 Selective Hydrogenation Applied to the Refining of Petrochemical Raw Materials Produced by Steam Cracking. In *Studies in Surface Science and Catalysis*; Cerveny, L., Ed.; Elsevier: Amsterdam, The Netherlands, 1986; Volume 27, pp. 613–666.
4. Puls, F.H.; Ruhnke, K.D. Butene-1 Containing Feed Purification Process (CS-165). U.S. Patent 4260840A, 7 April 1981.
5. Argyle, M.D.; Bartholomew, C.H. Heterogeneous catalyst deactivation and regeneration: A review. *Catalysts* **2015**, *5*, 145–269. [[CrossRef](#)]
6. Albers, P.; Pietsch, J.; Parker, S.F. Poisoning and deactivation of palladium catalysts. *J. Mol. Catal. A Chem.* **2001**, *173*, 275–286. [[CrossRef](#)]
7. Burger, B.J.; Thompson, M.E.; Cotter, W.D.; Bercaw, J.E. Ethylene insertion and beta-hydrogen elimination for permethylscandocene alkyl complexes. A study of the chain propagation and termination steps in Ziegler-Natta polymerization of ethylene. *J. Am. Chem. Soc.* **1990**, *112*, 1566–1577. [[CrossRef](#)]
8. Campos, K.R.; Cai, D.; Journet, M.; Kowal, J.J.; Larsen, R.D.; Reider, P.J. Controlled Semihydrogenation of Aminoalkynes Using Ethylenediamine as a Poison of Lindlar's Catalyst. *J. Org. Chem.* **2001**, *66*, 3634–3635. [[CrossRef](#)]
9. Lu, F.; Xu, Y.; Jiang, X.; Liu, Y.; Huang, J.; Sun, D. Biosynthesized Pd/ $\gamma$ -Al<sub>2</sub>O<sub>3</sub> catalysts for low-temperature 1,3-butadiene hydrogenation: The effect of calcination atmosphere. *New J. Chem.* **2017**, *41*, 13036–13042. [[CrossRef](#)]
10. Lu, F.; Sun, D.; Jiang, X. Plant-mediated synthesis of AgPd/ $\gamma$ -Al<sub>2</sub>O<sub>3</sub> catalysts for selective hydrogenation of 1,3-butadiene at low temperature. *New J. Chem.* **2019**, *43*, 13891–13898. [[CrossRef](#)]
11. Nikolaev, S.A.; Krotova, I.N. Partial hydrogenation of phenylacetylene over gold- and palladium-containing catalysts. *Pet. Chem.* **2013**, *53*, 394–400. [[CrossRef](#)]
12. Zhang, Q.; Li, J.; Liu, X.; Zhu, Q. Synergetic effect of Pd and Ag dispersed on Al<sub>2</sub>O<sub>3</sub> in the selective hydrogenation of acetylene. *Appl. Catal. A Gen.* **2000**, *197*, 221–228. [[CrossRef](#)]
13. Studt, F.; Abild-Pedersen, F.; Bligaard, T.; Sørensen, R.Z.; Christensen, C.H.; Nørskov, J.K. Identification of non-precious metal alloy catalysts for selective hydrogenation of acetylene. *Science* **2008**, *320*, 1320–1322. [[CrossRef](#)]
14. Totarella, G.; Beerthuis, R.; Masoud, N.; Louis, C.; Delannoy, L.; de Jongh, P.E. Supported Cu Nanoparticles as Selective and Stable Catalysts for the Gas Phase Hydrogenation of 1,3-Butadiene in Alkene-Rich Feeds. *J. Phys. Chem. C* **2021**, *125*, 366–375. [[CrossRef](#)] [[PubMed](#)]
15. Zhao, W.; Brouri, D.; Casale, S.; Delannoy, L.; Louis, C. Exploration of the preparation of Cu/TiO<sub>2</sub> catalysts by deposition-precipitation with urea for selective hydrogenation of unsaturated hydrocarbons. *J. Catal.* **2016**, *340*, 95–106.
16. Shi, X.; Lin, Y.; Huang, L.; Sun, Z.; Yang, Y.; Zhou, X.; Vovk, E.; Liu, X.; Huang, X.; Sun, M.; et al. Copper Catalysts in Semihydrogenation of Acetylene: From Single Atoms to Nanoparticles. *ACS Catal.* **2020**, *10*, 3495–3504. [[CrossRef](#)]
17. Huang, F.; Deng, Y.; Chen, Y.; Cai, X.; Peng, M.; Jia, Z.; Xie, J.; Xiao, D.; Wen, X.; Wang, N.; et al. Anchoring Cu<sub>1</sub> species over nanodiamond-graphene for semi-hydrogenation of acetylene. *Nat. Commun.* **2019**, *10*, 4431. [[CrossRef](#)] [[PubMed](#)]
18. Louis, C.; Delannoy, L. Chapter One—Selective hydrogenation of polyunsaturated hydrocarbons and unsaturated aldehydes over bimetallic catalysts. In *Advances in Catalysis*; Song, C., Ed.; Academic Press: Cambridge, MA, USA, 2019; Volume 64, pp. 1–88.
19. Xiaoke, H.; Xiaoyun, L.; Zhao, W.; Nian, H.; Zhao, D.; Lihua, C.; Baolian, S. Self-reduction for the Synthesis of Co Supported on Hierarchically Porous Carbon for Selective Hydrogenation Reaction. *Chem. J. Chin. Univ.* **2020**, *41*, 639–945. [[CrossRef](#)]
20. Wang, Z.; Wang, G.; Louis, C.; Delannoy, L. Bimetallic Ni–Zn/TiO<sub>2</sub> catalysts for selective hydrogenation of alkyne and alkydiene impurities from alkenes stream. *Res. Chem. Intermed.* **2021**, *47*, 91–116. [[CrossRef](#)]
21. Cao, Y.; Zhang, H.; Ji, S.; Sui, Z.; Jiang, Z.; Wang, D.; Zaera, F.; Zhou, X.; Duan, X.; Li, Y. Adsorption Site Regulation to Guide Atomic Design of Ni–Ga Catalysts for Acetylene Semi-Hydrogenation. *Angew. Chem. Int. Ed.* **2020**, *59*, 11647–11652. [[CrossRef](#)] [[PubMed](#)]
22. Putro, W.S.; Kojima, T.; Hara, T.; Ichikuni, N.; Shimazu, S. Selective hydrogenation of unsaturated carbonyls by Ni–Fe-based alloy catalysts. *Catal. Sci. Technol.* **2017**, *7*, 3637–3646. [[CrossRef](#)]
23. Hu, Q.; Wang, S.; Gao, Z.; Li, Y.; Zhang, Q.; Xiang, Q.; Qin, Y. The precise decoration of Pt nanoparticles with Fe oxide by atomic layer deposition for the selective hydrogenation of cinnamaldehyde. *Appl. Catal. B Environ.* **2017**, *218*, 591–599. [[CrossRef](#)]
24. Wehrli, J.T.; Thomas, D.J.; Wainwright, M.S.; Trimm, D.L.; Cant, N.W. Selective hydrogenation of propyne over supported copper catalysts: Influence of support. *Appl. Catal.* **1991**, *70*, 253–262. [[CrossRef](#)]
25. Stammbach, M.; Thomas, D.; Trimm, D.; Wainwright, M. Hydrogenation of ethyne over an ion-exchanged copper on silica catalyst. *Appl. Catal.* **1990**, *58*, 209–217. [[CrossRef](#)]



26. Ossipoff, N.J.; Cant, N. The hydrogenation and oligomerization of propyne over an ion-exchanged copper on silica catalyst. *J. Catal.* **1994**, *148*, 125–133. [[CrossRef](#)]
27. Sárkány, A.; Gucci, L.; Weiss, A.H. On the aging phenomenon in palladium catalysed acetylene hydrogenation. *Appl. Catal.* **1984**, *10*, 369–388. [[CrossRef](#)]
28. Sankar, M.; Dimitratos, N.; Miedziak, P.J.; Wells, P.P.; Kiely, C.J.; Hutchings, G.J. Designing bimetallic catalysts for a green and sustainable future. *Chem. Soc. Rev.* **2012**, *41*, 8099–8139. [[CrossRef](#)] [[PubMed](#)]
29. Delannoy, L.; Thrimurthulu, G.; Reddy, P.S.; Méthivier, C.; Nelayah, J.; Reddy, B.M.; Ricolleau, C.; Louis, C. Selective hydrogenation of butadiene over TiO<sub>2</sub> supported copper, gold and gold–copper catalysts prepared by deposition–precipitation. *Phys. Chem. Chem. Phys.* **2014**, *16*, 26514–26527. [[CrossRef](#)] [[PubMed](#)]
30. McCue, A.J.; McRitchie, C.J.; Shepherd, A.M.; Anderson, J.A. Cu/Al<sub>2</sub>O<sub>3</sub> catalysts modified with Pd for selective acetylene hydrogenation. *J. Catal.* **2014**, *319*, 127–135. [[CrossRef](#)]
31. Boucher, M.B.; Zugic, B.; Cladaras, G.; Kammert, J.; Marcinkowski, M.D.; Lawton, T.J.; Sykes, E.C.H.; Flytzani-Stephanopoulos, M. Single atom alloy surface analogs in Pd 0.18 Cu 15 nanoparticles for selective hydrogenation reactions. *Phys. Chem. Chem. Phys.* **2013**, *15*, 12187–12196. [[CrossRef](#)] [[PubMed](#)]
32. McCue, A.J.; Shepherd, A.M.; Anderson, J.A. Optimisation of preparation method for Pd doped Cu/Al<sub>2</sub>O<sub>3</sub> catalysts for selective acetylene hydrogenation. *Catal. Sci. Technol.* **2015**, *5*, 2880–2890. [[CrossRef](#)]
33. Lucci, F.R.; Liu, J.; Marcinkowski, M.D.; Yang, M.; Allard, L.F.; Flytzani-Stephanopoulos, M.; Sykes, E.C.H. Selective hydrogenation of 1, 3-butadiene on platinum-copper alloys at the single-atom limit. *Nat. Commun.* **2015**, *6*, 8550. [[CrossRef](#)]
34. Zhao, W.; Wang, G.; Louis, C.; Delannoy, L. Novel non-noble bimetallic Cu-Zn/TiO<sub>2</sub> catalysts for selective hydrogenation of butadiene. *J. Catal.* **2017**, *347*, 185–196.
35. Zhao, Y.; Guo, Z.; Zhang, H.; Peng, B.; Xu, Y.; Wang, Y.; Zhang, J.; Xu, Y.; Wang, S.; Ma, X. Hydrogenation of diesters on copper catalyst anchored on ordered hierarchical porous silica: Pore size effect. *J. Catal.* **2018**, *357*, 223–237. [[CrossRef](#)]
36. Hu, N.; Li, X.-Y.; Liu, S.-M.; Wang, Z.; He, X.-K.; Hou, Y.-X.; Wang, Y.-X.; Deng, Z.; Chen, L.-H.; Su, B.-L. Enhanced stability of highly-dispersed copper catalyst supported by hierarchically porous carbon for long term selective hydrogenation. *Chin. J. Catal.* **2020**, *41*, 1081–1090. [[CrossRef](#)]
37. Su, B.L.; Vantomme, A.; Surahy, L.; Pirard, R.; Pirard, J.P. Hierarchical Multimodal Mesoporous Carbon Materials with Parallel Macrochannels. *Chem. Mater.* **2007**, *19*, 3325–3333. [[CrossRef](#)]
38. Yuan, Z.Y.; Ren, T.Z.; Azioune, A.; Pireaux, J.J.; Su, B.L. Self-Assembly of Hierarchically Mesoporous–Macroporous Phosphated Nanocrystalline Aluminum (Oxyhydr)oxide Materials. *Chem. Mater.* **2006**, *18*, 1753–1767. [[CrossRef](#)]
39. Dapsens, P.Y.; Hakim, S.H.; Su, B.-L.; Shanks, B.H. Direct observation of macropore self-formation in hierarchically structured metal oxides. *Chem. Commun.* **2010**, *46*, 8980–8982. [[CrossRef](#)]
40. Zanella, R.; Delannoy, L.; Louis, C. Mechanism of deposition of gold precursors onto TiO<sub>2</sub> during the preparation by cation adsorption and deposition–precipitation with NaOH and urea. *Appl. Catal. A Gen.* **2005**, *291*, 62–72. [[CrossRef](#)]
41. Cychosz, K.A.; Guillet-Nicolas, R.; García-Martínez, J.; Thommes, M. Recent advances in the textural characterization of hierarchically structured nanoporous materials. *Chem. Soc. Rev.* **2017**, *46*, 389–414. [[CrossRef](#)]
42. Chen, M.; Wang, J.; Jiang, B.; Yang, Y. Diffusion measurements of isopentane, 1-hexene, cyclohexane in polyethylene particles by the intelligent gravimetric analyzer. *J. Appl. Polym. Sci.* **2013**, *127*, 1098–1104. [[CrossRef](#)]
43. Huang, H.H.; Yan, F.Q.; Kek, Y.M.; Chew, C.H.; Xu, G.Q.; Ji, W.; Oh, P.S.; Tang, S.H. Synthesis, Characterization, and Nonlinear Optical Properties of Copper Nanoparticles. *Langmuir* **1997**, *13*, 172–175. [[CrossRef](#)]
44. Condorelli, G.G.; Costanzo, L.L.; Fragalà, I.L.; Giuffrida, S.; Ventimiglia, G. A single photochemical route for the formation of both copper nanoparticles and patterned nanostructured films. *J. Mater. Chem.* **2003**, *13*, 2409–2411. [[CrossRef](#)]
45. Savinova, E.R.; Chuvilin, A.L.; Parmon, V.N. Copper colloids stabilized by water-soluble polymers: Part I. Preparation and properties. *J. Mol. Catal.* **1988**, *48*, 217–229. [[CrossRef](#)]
46. Derrouiche, S.; La Fontaine, C.; Thrimurtulu, G.; Casale, S.; Delannoy, L.; Lauron-Pernot, H.; Louis, C. Unusual behaviour of Au/ZnO catalysts in selective hydrogenation of butadiene due to the formation of a AuZn nanoalloy. *Catal. Sci. Technol.* **2016**, *6*, 6794–6805. [[CrossRef](#)]
47. Miyazaki, M.; Furukawa, S.; Takayama, T.; Yamazoe, S.; Komatsu, T. Surface Modification of PdZn Nanoparticles via Galvanic Replacement for the Selective Hydrogenation of Terminal Alkynes. *ACS Appl. Nano Mater.* **2019**, *2*, 3307–3314. [[CrossRef](#)]
48. Sun, M.-H.; Huang, S.-Z.; Chen, L.-H.; Li, Y.; Yang, X.-Y.; Yuan, Z.-Y.; Su, B.-L. Applications of hierarchically structured porous materials from energy storage and conversion, catalysis, photocatalysis, adsorption, separation, and sensing to biomedicine. *Chem. Soc. Rev.* **2016**, *45*, 3479–3563. [[CrossRef](#)]
49. Wang, Z. Selective Hydrogenation of Butadiene over Non-Noble Bimetallic Catalysts. (Catalyseurs Bimétalliques à Base de Métaux Non Nobles Pour L’hydrogénation Sélective du Butadiène—Paris VI). Ph.D. Thesis, Université Pierre et Marie Curie, Paris, France, 2017.
50. Wiame, F.; Islam, M.M.; Salgın, B.; Światowska, J.; Costa, D.; Diawara, B.; Maurice, V.; Marcus, P. Zn effect on STM imaging of brass surfaces. *Surf. Sci.* **2016**, *644*, 148–152. [[CrossRef](#)]
51. Krajčič, M.; Hafner, J. Intermetallic Compounds as Selective Heterogeneous Catalysts: Insights from DFT. *ChemCatChem* **2016**, *8*, 34–48. [[CrossRef](#)]

52. Bridier, B.; López, N.; Pérez-Ramírez, J. Molecular understanding of alkyne hydrogenation for the design of selective catalysts. *Dalton Trans.* **2010**, *39*, 8412–8419. [[CrossRef](#)] [[PubMed](#)]
53. Berteau, P.; Ceckiewicz, S.; Delmon, B. Role of the acid-base properties of aluminas, modified  $\gamma$ -alumina, and silica-alumina in 1-butanol dehydration. *Appl. Catal.* **1987**, *31*, 361–383. [[CrossRef](#)]
54. Hugon, A.; Delannoy, L.; Louis, C. Supported gold catalysts for selective hydrogenation of 1,3-butadiene in the presence of an excess of alkenes. *Gold Bull.* **2008**, *41*, 127–138. [[CrossRef](#)]
55. Catillon-Mucherie, S.; Ammari, F.; Krafft, J.-M.; Lauron-Pernot, H.; Touroude, R.; Louis, C. Preparation of Coimpregnated Cu–Zn/SiO<sub>2</sub> Catalysts: Influence of the Drying Step on Metallic Particle Size and on Cu<sup>0</sup>–ZnII Interactions. *J. Phys. Chem. C* **2007**, *111*, 11619–11626. [[CrossRef](#)]